SOFT ROBOTICS
Volume 1, Number 2, 2014

DOI: 10.1089/soro.2013.0011

SoRo
Soft Robotics

ORIGINAL ARTICLE

Theoretical Modeling and Experimental Analysis of a Pressure-Operated Soft Robotic Snake

Ming Luo,[1,2] Mahdi Agheli,[3] and Cagdas D. Onal[1,3]

Abstract

For a mobile robot undergoing serpentine locomotion, an accurate dynamic model is a fundamental requirement for optimization, control, navigation, and learning algorithms. Such algorithms can be readily implemented for traditional rigid robots, but remain a challenge for nonlinear and low-bandwidth soft robotic systems. This article addresses the theoretical modeling of the dynamics of a pressure-operated soft snake robot. A general framework is detailed to solve the 2D modeling problem of a soft snake robot, which is applicable to most pressure-operated soft robots developed by a modular kinematic arrangement of bending-type fluidic elastomer actuators. The model is simulated using measured physical parameters of a soft snake robot prototype. The theoretical results are verified through a detailed comparison to locomotion experiments on a flat surface with measured frictional properties. Experimental results confirm that the proposed model describes the motion of the robot accurately.

Introduction

Robots offer great promise in assisting search-and-rescue operations in extremely hostile environments after a variety of accidents. In such applications, robots need to navigate through constrained environments such as inside narrow pipes or over debris. Locomotion under these conditions requires special robotic capabilities that may not be fulfilled by traditional mobile robots. A robotic snake is a salient solution for such conditions since it can navigate on unstructured terrain without limbs while being able to pass through narrow openings or complex passages, similar to its biological counterpart.

Many researchers studied the principles of snake locomotion and developed robotic equivalents that can replicate snake motion. The first snake robot was developed by Shigeo Hirose in 1971.[1] During 40 years of research, many snake robots have been developed, including Anna Konda, a large firefighting snake; Aiko, a portable system for experimentation; and Pneumosnake, a system developed to investigate joint actuation based on pneumatic bellows.[2] More recent research on robotic snake-like locomotion has studied a new approach using a toroidal skin drive system to continuously propel the body of the robot forward and improve performance.[3] Sato *et al*.,[4] Fjerdingen *et al*.,[5] and Shugen[6] studied modeling a rigid snake robot in 2D. Pettersen[7] added expressions for the linear velocity of individual links based on previous work and divided the general model into an actuated and an un-actuated part. Subsequently, partial feedback linearization of the model was presented. In addition, Patterson proposed a simplified model after linearization and gave proofs of stability and controllability of a rigid snake robot based on the proposed model. Matsuno *et al.*,[8] Tanaka *et al.*,[9] and Transeth *et al.*[10] studied segmented rigid snake robot modeling in 3D by taking vertical motions into account.

Although many snake robots have been developed, current approaches do not utilize body flexibility. Since traditional robot fabrication is based on rigid links, robotic snakes may not be as safe and adaptive as their natural counterparts. Our objective in this research was to develop a pressure-operated soft robotic snake that can overcome the limitations of rigid snake robots. Soft robotics has recently seen a flurry of research as well as many different kinds of crawling robots.[1,11–18] However, mathematical modeling of soft robots has been limited since the deformable nature of such systems creates a challenge such that a soft body may create infinite degrees of freedom. Xydas *et al.*[19] and Ilievski *et al.*[20] showed that finite element analysis can be utilized to model soft robots. However, this method focuses on the selection of material and not on the whole dynamic motion.

The first generation of our soft robotic snake was developed by Onal and Rus.[21,22] The body is fabricated by molding

[1]Robotics Engineering Program and [3]Department of Mechanical Engineering, Worcester Polytechnic Institute, Worcester, Massachusetts.
[2]School of Computer and Information, AnQing Normal University, Anhui, China.

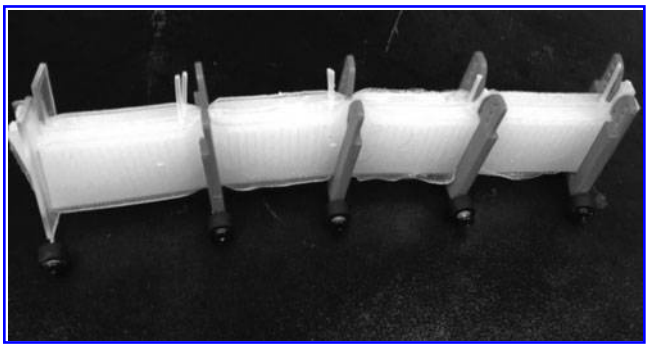

FIG. 1. Experimental prototype of our pressure-operated soft robotic snake, comprising four bidirectional fluidic elastomer actuators connected in series as segments and passive wheels to create the required frictional anisotropy for undulatory serpentine locomotion.

silicone rubber in three layers. The total manufacturing and assembly process takes 14 h from scratch, resulting in an inexpensive robot. A recent prototype of our fluidic soft robot is shown in Figure 1. Some challenges with the first generation of the snake robot included the need for an accurate model for deeper research in optimization and algorithms, a perception system for gait control, and a skin that offers anisotropic friction for eliminating the passive wheels, which is a current problem in snake robots in general. This article focuses on the first challenge, that is, accurate modeling of the robot. In previous works, we utilized a fundamental constant curvature kinematic model and augmented an anisotropic friction function to iteratively describe the shape of the body over time and provide a general intuition about the locomotion of our soft snake robot.[22] In this work, we take a more detailed and systematic approach to theoretical modeling, treating each soft segment as a joint, and short solid connectors between segments as links.[23] This approach is compatible with existing rigid snake robot dynamic modeling studies and provides an accurate description of the whole system.

The rest of the article is organized as follows: the Theoretical Modeling section shows the mathematical details of the soft snake robot model. The Results section displays the results including the fabrication of the robot, dynamic simulation studies of the theoretical model, and a comparison between simulated and experimental results. The Conclusion section includes a discussion on future research.

Theoretical Modeling

This section details the kinematic and dynamic model of our soft robotic snake. We first present a complete model that takes the length of connectors between segments into account. These connectors occur practically because of solid silicone strips as well as valve and passive wheel holders between individual segment actuators.[22] The complete model is then simplified with the assumption of zero-length connectors to achieve a continuous soft robotic chain for ease of simulations.

Complete model

A general soft snake robot comprises N rigid links of length $2l_1$ and $N-1$ soft segments (joints) of length l_2. All N links have the same moment of inertia J and mass m. We assume that the link center of mass (CoM) is located at the geometric center of each link. Table 1 lists all the mathematical parameters of the kinematics and dynamics model, which are also graphically depicted in Figure 2.

The soft snake robot works on a 2D surface. The following definitions are illustrated similar to a rigid snake robot[7]:

Definition 1 (link angle): The link angle of link $i \in (1, \ldots, N) \in \Re^N$ of the snake robot is noted by $\theta_i \in \Re$ with respect to the global x-axis with counterclockwise positive direction.

Definition 2 (curvature): The curvature of joint $i \in (1, \ldots, N-1) \in \Re^{N-1}$ of the snake robot is noted by $\kappa_i \in \Re$, which is defined as:[22]

$$\kappa_i = \frac{\theta_i - \theta_{i+1}}{l_2}. \tag{1}$$

Given a bidirectional bending module i of length l_2, out of $N-1$ modules in

Definition 3 (the global position): The position of the robot with respect to the global frame $\boldsymbol{p} \in \Re^2$ is given by:

$$\boldsymbol{p} = \begin{pmatrix} p_x \\ p_y \end{pmatrix} = \begin{pmatrix} \frac{1}{Nm}\sum_{i=1}^{N} mx_i \\ \frac{1}{Nm}\sum_{i=1}^{N} my_i \end{pmatrix} = \frac{1}{N}\begin{pmatrix} \boldsymbol{e}^T\mathbf{X} \\ \boldsymbol{e}^T\mathbf{Y} \end{pmatrix}, \tag{2}$$

where the vectors: $\mathbf{X} = (x_1, \ldots x_N)^T \in \Re^N$, $\mathbf{Y} = (y_1, \ldots, y_N)^T \in \Re^N$, and $\mathbf{e} = (1, \ldots, 1)^T \in \Re^N$.

Table 1. Parameters of the Soft Robotic Snake Model

Symbol	*Description*	*Vector*
N	The number of links	
l_1	Half the length of the rigid link	
l_2	The length of the rigid link	
m	Mass of each link	
ΔS	The bottom area of the soft actuator	
J	Moment of inertia of each link	
U_t	The friction factor in the tangential direction	
U_n	The friction factor in the normal direction	
θ_i	Angle between link i and the global x-axis	$\theta \in \Re^{\mathbf{N}}$
κi	Curvature of each link	$\kappa \in \Re^{\mathbf{N}}$
$(x_i\ y_i)$	Global coordinates of the CoM of link i	$\mathbf{X}, \mathbf{Y} \in \Re^{\mathbf{N}}$
$(p_i\ p_y)$	Global coordinates of the CoM of the robot i	$\mathbf{p} \in \Re^{\mathbf{2}}$
P_i	Pressure input on joint i	$\mathbf{P} \in \Re^{\mathbf{N-1}}$
P_{i-1}	Pressure input on joint i - 1	$\mathbf{P} \in \Re^{\mathbf{N-1}}$
$(f_{R,x,i}, f_{R,y,i})$	Ground friction force on link i	$\mathbf{f_{R,x}}, \mathbf{f_{R,y}} \in \Re^{\mathbf{N}}$
$(h_{x,i}, h_{y,i})$	Joint constraint force on link i from link $i+1$	$\mathbf{h_x}, \mathbf{h_y} \in \Re$
$(h_{x,i-1}, h_{y,i})$	Joint constraint force on link i from link $i-1$	$\mathbf{h_x}, \mathbf{h_y} \in \Re^{\mathbf{N}}$

CoM, center of mass.

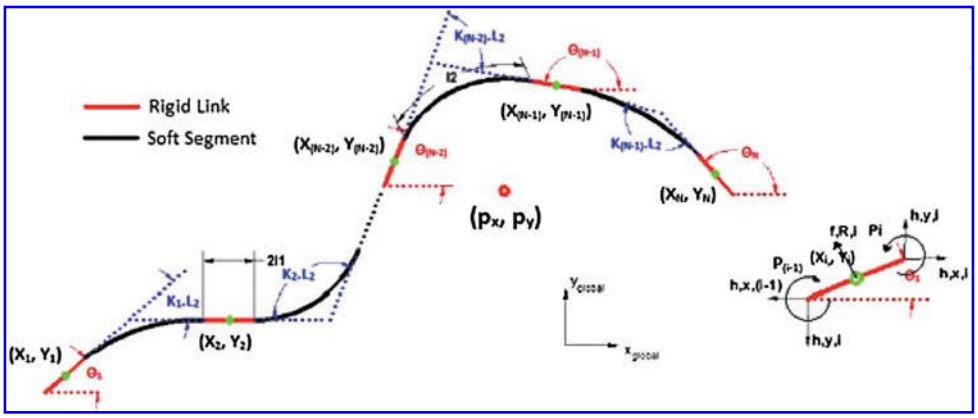

FIG. 2. The complete model of a soft robotic snake includes short rigid links connected together with soft bending segments. Color images available online at www.liebertpub.com/soro

The position difference between two neighbor links has two parts: the rigid link and the soft segment. The position relationship of all links is written as:

$$\begin{aligned} \mathbf{DX} + l_1\mathbf{A}\cos\boldsymbol{\theta} + l_2 diag(\mathbf{D}\sin\boldsymbol{\theta})\bar{\boldsymbol{\kappa}} = 0, \\ \mathbf{DY} + l_1\mathbf{A}\sin\boldsymbol{\theta} - l_2 diag(\mathbf{D}\cos\boldsymbol{\theta})\bar{\boldsymbol{\kappa}} = 0, \end{aligned} \tag{3}$$

where $\mathbf{A} = \begin{pmatrix} 1 & 1 & & \\ & \ddots & \ddots & \\ & & 1 & 1 \end{pmatrix} \in \Re^{(N-1)\times N}$, $\mathbf{D} = \begin{pmatrix} 1 & -1 & & \\ & \ddots & \ddots & \\ & & 1 & -1 \end{pmatrix} \in \Re^{(N-1)\times N}$, and $\bar{\boldsymbol{\kappa}} = \left(\frac{1}{\kappa_1}, \ldots, \frac{1}{\kappa_N}\right)^T \in \Re^{N-1}$.

Combining Equations 3 and 4, the center position of each link is given as:

$$\begin{aligned} \mathbf{X} &= -l_1\mathbf{K}^{\mathbf{T}}\mathbf{A}\cos\boldsymbol{\theta} - l_2\mathbf{Z}diag(\mathbf{D}\sin\boldsymbol{\theta})\bar{\kappa} + \mathbf{e}p_x \\ \mathbf{Y} &= -l_1\mathbf{K}^{\mathbf{T}}\mathbf{A}\sin\boldsymbol{\theta} + l_2\mathbf{Z}diag(\mathbf{D}\cos\boldsymbol{\theta})\bar{\kappa} + \mathbf{e}p_y \end{aligned}, \tag{4}$$

where $\mathbf{Z} = \mathbf{D}^T(\mathbf{D}\mathbf{D}^T)^{-1} \in \Re^{N\times N-1}$ and $\mathbf{K} = \mathbf{A}^T(\mathbf{D}\mathbf{D}^T)^{-1}\mathbf{D} \in \Re^{N\times N}$.

The soft snake robot can undulate forward with the help of ground friction forces. In this work we use Coulomb friction model as:

$$\begin{aligned} \mathbf{f_R} &= \begin{pmatrix} \mathbf{f_{R,x}} \\ \mathbf{f_{R,y}} \end{pmatrix} \\ &= -mg\begin{pmatrix} U_t\mathbf{C_\theta} & -U_n\mathbf{S_\theta} \\ U_t\mathbf{S_\theta} & U_n\mathbf{C_\theta} \end{pmatrix} \mathrm{sgn}\left(\begin{pmatrix} \mathbf{C_\theta} & \mathbf{S_\theta} \\ -\mathbf{S_\theta} & \mathbf{C_\theta} \end{pmatrix}\begin{pmatrix} \dot{\mathbf{X}} \\ \dot{\mathbf{Y}} \end{pmatrix}\right), \end{aligned} \tag{5}$$

where $\mathbf{S_\theta} = \mathrm{diag}(\sin\boldsymbol{\theta}) \in \Re^{N\times N}$ *and* $\mathbf{C_\theta} = diag(\cos\boldsymbol{\theta}) \in \Re^{N\times N}$.

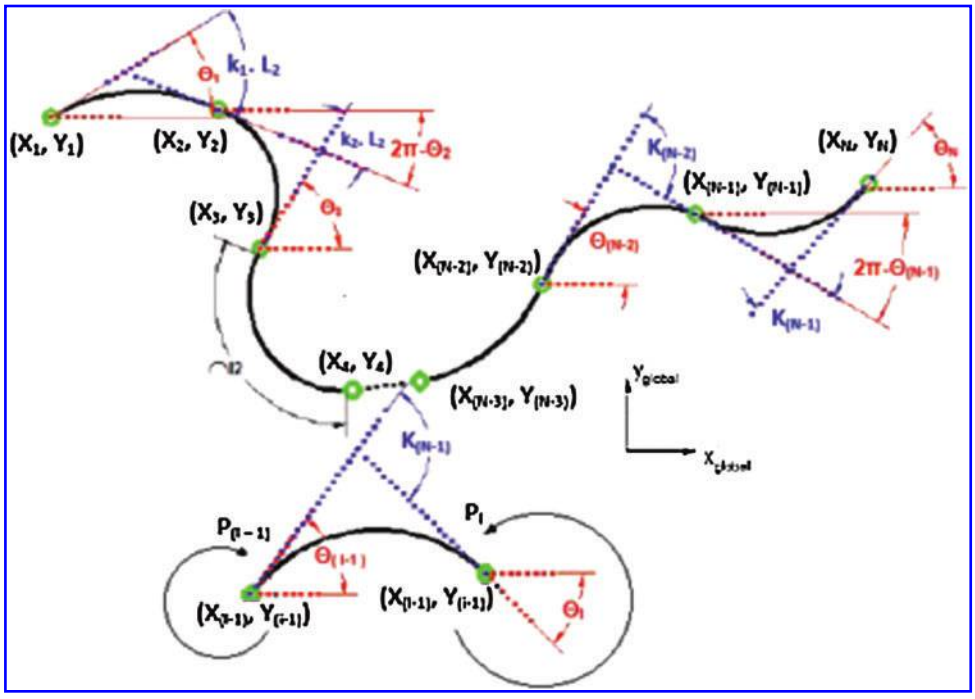

FIG. 3. The simplified model of the soft snake robot that assumes zero-length links between bending joints (segments). Color images available online at www.liebertpub.com/soro

Figure 2 depicts the force balance on each link. The ground friction force and joint constraint force both have influence on the dynamics of the soft snake robot. According to Newton's law, the force balance equations are given as:

$$\begin{aligned} m\ddot{\mathbf{X}} &= \mathbf{f_{R,x}} + \mathbf{D}^T\mathbf{h}_x, \\ m\ddot{\mathbf{Y}} &= \mathbf{f_{R,y}} + \mathbf{D}^T\mathbf{h}_y, \end{aligned} \tag{6}$$

where $\mathbf{h_x} = (h_{x,1}, \ldots, h_{x,N})^T \in \Re^N$ and $\mathbf{h_y} = (h_{y,1}, \ldots, h_{y,N})^T \in \Re^N$.

Similarly, the torque balance for all links is given as:

$$J\ddot{\boldsymbol{\theta}} = \Delta S l_2 \mathbf{D}^T\mathbf{P} - l_1\mathbf{S_\theta}\mathbf{A}^T\mathbf{h_x} + l_1\mathbf{C_\theta}\mathbf{A}^T\mathbf{h_y}. \tag{7}$$

Taking the first and second derivatives of Equation 5, we can plug expressions into Equations 6 and 7 and finally combine Equation 8 to yield:

$$\begin{aligned} &\mathbf{M_\theta}\ddot{\boldsymbol{\theta}} + \mathbf{W}\dot{\boldsymbol{\theta}}^2 + \mathbf{T}\dot{\boldsymbol{\theta}} + \mathbf{Y}\ddot{\boldsymbol{\kappa}} + \mathbf{Q} - l_1\mathbf{S_\theta}\mathbf{K}^\mathbf{T}\mathbf{f_{R,X}} + l_1\mathbf{C_\theta}\mathbf{K}^\mathbf{T}\mathbf{f_{y,R}} \\ &\quad = \Delta S l_2 \mathbf{D}^\mathbf{T}\mathbf{P} \\ &Nm\ddot{\mathbf{P}} = \mathbf{E}^\mathbf{T}\mathbf{f_R}, \end{aligned} \tag{8}$$

where

$$\begin{aligned} \mathbf{M_\theta} &= \mathbf{JI_N} + ml_1^2\mathbf{S_\theta}\mathbf{V}\mathbf{S_\theta} + ml_1^2\mathbf{C_\theta}\mathbf{V}\mathbf{C_\theta} - ml_1l_2\mathbf{S_\theta}\mathbf{Z}\mathbf{B_1} \\ &\quad - ml_1l_2\mathbf{C_\theta}\mathbf{Z}\mathbf{B_2}, \\ W_\theta &= ml_1^2\mathbf{S_\theta}\mathbf{V}\mathbf{C_\theta} - ml_1^2\mathbf{C_\theta}\mathbf{V}\mathbf{S_\theta} - ml_1l_2\mathbf{S_\theta}\mathbf{Z}\mathbf{B_2} + ml_1l_2\mathbf{C_\theta}\mathbf{Z}\mathbf{B_1}, \\ \mathbf{T_\theta} &= -ml_1l_2\mathbf{S_\theta}\mathbf{Z}\mathbf{B_3} - ml_1l_2\mathbf{C_\theta}\mathbf{Z}\mathbf{B_6}, \\ \mathbf{Q_\theta} &= -ml_1l_2\mathbf{S_\theta}\mathbf{Z}\mathbf{B_4} - ml_1l_2\mathbf{C_\theta}\mathbf{Z}\mathbf{B_7}, \\ Y_\theta &= -ml_1l_2\mathbf{S_\theta}\mathbf{Z}\mathbf{B_5} - ml_1l_2\mathbf{C_\theta}\mathbf{Z}\mathbf{B_8}, \end{aligned} \tag{9}$$

for vectors $\mathbf{V} = \mathbf{A}^\mathbf{T}(\mathbf{D}\mathbf{D}^\mathbf{T})^{-1}\mathbf{A} \in \Re^{N\times N}$ and $\mathbf{E} = \begin{pmatrix} \mathbf{e} & \mathbf{0_{N\times 1}} \\ \mathbf{0_{N\times 1}} & \mathbf{e} \end{pmatrix} \in \Re^{2N\times 2}$.

Equations 11–13 describe the format of the matrices $\mathbf{B_1}$ through $\mathbf{B_8}$ for the given $C_{j,k}$ elements for each case:

$$\mathbf{B_1} = \mathbf{F_1} \text{ with } C_{1,2i-1} = \frac{cos\theta_i}{\kappa_i} \text{ and } C_{1,2i} = -\frac{cos\theta_{i+1}}{\kappa_i}$$

$$\mathbf{B_2} = \mathbf{F_1} \text{ with } C_{1,2i-1} = -\frac{sin\theta_i}{\kappa_i} \text{ and } C_{1,2i} = \frac{sin\theta_{i+1}}{\kappa_i}$$

$$\mathbf{B_3} = \mathbf{F_1} \text{ with } C_{1,2i-1} = -\frac{\kappa_i^2 cos\theta_i}{\kappa_i} \text{ and } C_{1,2i} = \frac{\kappa_i^2 cos\theta_{i+1}}{\kappa_i}$$

$$\mathbf{B_4} = \mathbf{F_2} \text{ with } C_{2,i} = \frac{\kappa_i^2(sin\theta_i - sin\theta_{i+1})}{\kappa_i^3}$$

$$\mathbf{B_5} = \mathbf{F_3} \text{ with } C_{3,i} = \frac{sin\theta_{i+1} - sin\theta_i}{\kappa_i^2}$$

$$\mathbf{B_6} = \mathbf{F_1} \text{ with } C_{1,2i-1} = \frac{\kappa_i sin\theta_i}{\kappa_i^2} \text{ and } C_{1,2i} = -\frac{\kappa_i sin\theta_{i+1}}{\kappa_i^2}$$

$$\mathbf{B_7} = \mathbf{F_2} \text{ with } C_{2,i} = \frac{\kappa_i^2(cos\theta_i - cos\theta_{i+1})}{\kappa_i^3}$$

$$\mathbf{B_8} = \mathbf{F_3} \text{ with } C_{3,i} = \frac{cos\theta_{i+1} - cos\theta_i}{\kappa_i^2}$$

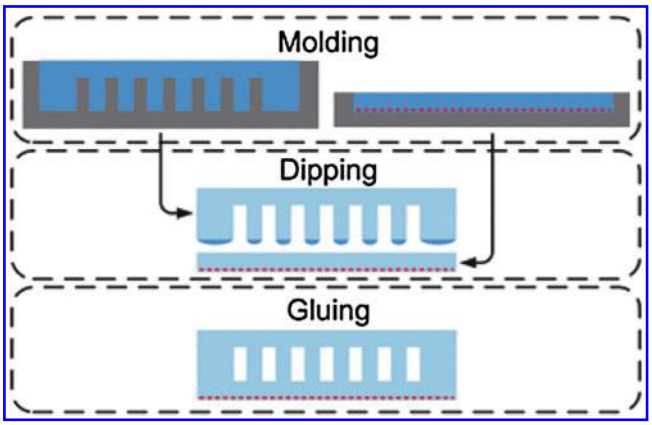

FIG. 4. Fabrication process of each segment of the soft robotic snake.[21] Color images available online at www.liebertpub.com/soro

$$\mathbf{F_1} = \begin{pmatrix} \mathbf{0_{0\times 0}} & \mathbf{C_{1,1}} & \mathbf{C_{1,2}} & \mathbf{0_{1\times N-2}} \\ \mathbf{0_{1\times 1}} & \mathbf{C_{1,3}} & \mathbf{C_{1,3}} & \mathbf{0_{1\times N-3}} \\ \cdot & \cdot & \cdot & \cdot \\ \cdot & \cdot & \cdot & \cdot \\ \cdot & \cdot & \cdot & \cdot \\ \mathbf{0_{1\times N-3}} & \mathbf{C_{1,2N-5}} & \mathbf{C_{1,2N-4}} & \mathbf{0_{1\times 1}} \\ \mathbf{0_{1\times N-2}} & \mathbf{C_{1,2N-3}} & \mathbf{C_{1,2N-2}} & \mathbf{0_{0\times 0}} \end{pmatrix} \in \Re^{(N-1)\times N} \tag{10}$$

$$\mathbf{F_2} = \mathbf{2}\begin{pmatrix} \mathbf{C_{2,1}} \\ \mathbf{C_{2,2}} \\ \cdot \\ \cdot \\ \cdot \\ \mathbf{C_{2,N-2}} \\ \mathbf{C_{N-1}} \end{pmatrix} \in \Re^{(N-1)\times 1} \tag{11}$$

$$\mathbf{F_3} = \begin{pmatrix} \mathbf{0_{0\times 0}} & \mathbf{C_{3,1}} & \mathbf{0_{1\times N-1}} \\ \mathbf{0_{1\times 1}} & \mathbf{C_{3,2}} & \mathbf{0_{1\times N-2}} \\ \cdot & \cdot & \cdot \\ \cdot & \cdot & \cdot \\ \cdot & \cdot & \cdot \\ \mathbf{0_{1\times N-2}} & \mathbf{C_{3,N-2}} & \mathbf{0_{1\times 1}} \\ \mathbf{0_{1\times N-1}} & \mathbf{C_{3,N-1}} & \mathbf{0_{0\times 0}} \end{pmatrix} \in \Re^{(N-1)\times N} \tag{12}$$

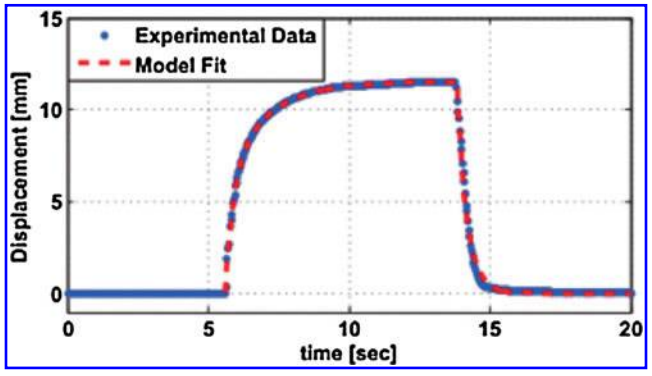

FIG. 5. Dynamic response of the fluidic elastomer actuators under a step pressure input.[22] Color images available online at www.liebertpub.com/soro

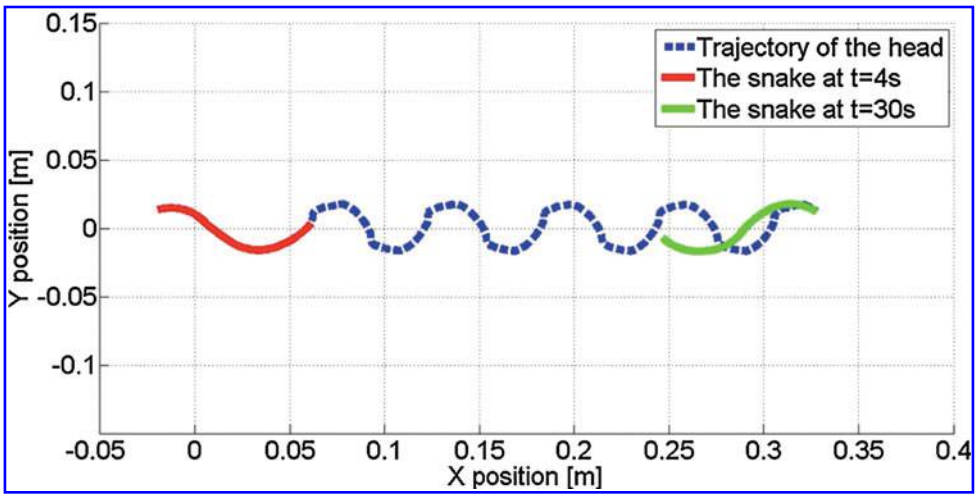

FIG. 6. Numerical simulation of the dynamic locomotion of a soft robotic snake, where the initial shape and the final shape of the body, as well as the trajectory of the head are indicated. Color images available online at www.liebertpub.com/soro

This set of equations provides an accurate mathematical representation of the dynamics of our soft snake robot. However, they are difficult to implement in a simulated environment because of computational costs. In what follows, we describe a simplification that leads to more tractable expressions that can be run more than 100 times faster than the complete model using Matlab ODE solver.

Simplified model

For simplicity and practical applications, the rigid link lengths (l_1) can be ignored as compared to the length of the soft segments (l_2). Figure 3 displays this simplified dynamics modeling approach for a fluidic soft snake robot graphically. With the zero link-length assumption, the position relationship for all links in Equation 4 becomes:

$$\begin{aligned} \mathbf{DX} + l_2 diag(\mathbf{D}\sin\boldsymbol{\theta})\bar{\boldsymbol{\kappa}} = \mathbf{0}, \\ \mathbf{DY} - l_2 diag(\mathbf{D}\cos\boldsymbol{\theta})\bar{\boldsymbol{\kappa}} = \mathbf{0}. \end{aligned} \tag{13}$$

The center position of links in Equation 5 can be rewritten as:

$$\begin{aligned} \mathbf{X} = -l_2\mathbf{Z}diag(\mathbf{D}\sin\boldsymbol{\theta})\bar{\boldsymbol{\kappa}} + \mathbf{e}p_x \\ \mathbf{Y} = l_2\mathbf{Z}diag(\mathbf{D}\cos\boldsymbol{\theta})\bar{\boldsymbol{\kappa}} + \mathbf{e}p_y. \end{aligned} \tag{14}$$

This simplified model of the soft snake robot has no rigid links, so in Equation 7, the joint constraint force term can be ignored, because the value of l_1 is set to be 0, simplifying the force balance relation as:

$$\begin{aligned} m\ddot{\mathbf{X}} = \mathbf{f}_{\mathbf{R},\mathbf{x}} \\ m\ddot{\mathbf{Y}} = \mathbf{f}_{\mathbf{R},\mathbf{Y}}. \end{aligned} \tag{15}$$

Similarly, the torque balance for all links in Equation 8 becomes:

$$\mathbf{J}\ddot{\boldsymbol{\theta}} = \Delta S l_2 \mathbf{D}^{\mathbf{T}}\mathbf{P}. \tag{16}$$

The combined dynamic motion expression in Equation 9 then becomes:

$$\begin{aligned} \mathbf{M}_{\boldsymbol{\theta}}\ddot{\boldsymbol{\theta}} = \Delta S l_2 \mathbf{D}^{\mathbf{T}}\mathbf{P} \\ Nm\mathbf{P} = \mathbf{E}^{\mathbf{T}}\mathbf{f}_{\mathbf{R}} \end{aligned}, \tag{17}$$

where $\mathbf{M}_{\theta} = \mathbf{J}\mathbf{I}_{\mathbf{N}}$.

Equation 18 describes the soft snake robot system as a whole. For convenience, the next step is separating the actuated and unactuated dynamics leading to direct dynamic relations of the position and orientation of the robot. Defining:

$$\begin{aligned} \mathbf{q}_{\boldsymbol{\kappa}} = \begin{pmatrix} \boldsymbol{\kappa}^* \\ \mathbf{p} \end{pmatrix} \in \Re^{N+2}, \\ \boldsymbol{\theta} = \mathbf{H}\boldsymbol{\kappa}^*, \end{aligned} \tag{18}$$

where $\boldsymbol{\kappa}^* = (\kappa_1, \ldots, \kappa_N\ \theta_N)^T \in \Re^N$ and

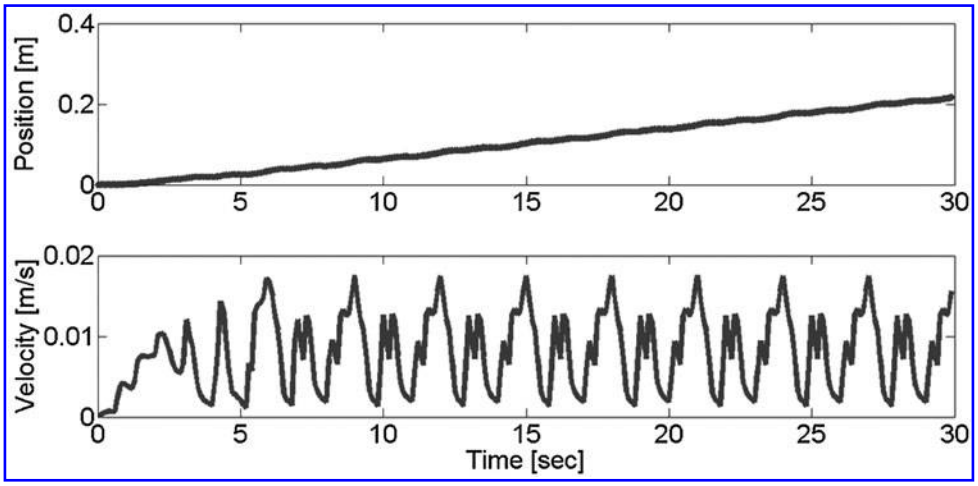

FIG. 7. Position and velocity of the simulated soft snake robot center of mass (CoM) over time for the numerical simulation results shown in Figure 6.

Table 2. Experimental Parameters

Symbol	*Description*	*Value*	*Unit*
N	The number of links	5	
G	The weight of each soft segment	0.25	kg
U_t	The friction factor in the tangential direction	0.0966	
U_n	The friction factor in the normal direction	0.68	
α	Amplitude	21	rad/mm
T	Undulation period	$\frac{2\pi}{3}$	rad/s

$$\mathbf{H} = \begin{pmatrix} 1 & 1 & 1 & \cdot & \cdot & \cdot & 1 & 1 \\ 0 & 1 & 1 & \cdot & \cdot & & 1 & 1 \\ \cdot & & & & & & & \cdot \\ \cdot & & & & & & & \cdot \\ \cdot & & & & & & & \cdot \\ 0 & 0 & 0 & \cdot & \cdot & \cdot & 0 & 1 \end{pmatrix} \in \Re^{N\times N} \tag{19}$$

Inserting Equation 20 into Equation 19, and premultiplying with $\mathbf{H^T}$ yields:

$$\mathbf{M^*_{\kappa^*}}\ddot{\mathbf{q}}_{\boldsymbol{\kappa}} + \mathbf{G^*_{\kappa^*}}\mathbf{f_R} = \Delta S l_2 \overline{\mathbf{B}}\mathbf{P}, \tag{20}$$

where $\mathbf{M^*_{\kappa^*}} = \begin{pmatrix} \mathbf{H^T}\mathbf{M}_\theta(\mathbf{k}^*) & \mathbf{0_{N\times 2}} \\ \mathbf{0_{2\times N}} & \mathbf{NmI_2} \end{pmatrix}$, $\mathbf{G^*_{\kappa^*}} = \begin{pmatrix} \mathbf{0^{1\times N}} & \mathbf{0^{1\times N}} \\ -\mathbf{e^T} & \mathbf{0^{1\times N}} \\ \mathbf{0^{1\times N}} & -\mathbf{e^T} \end{pmatrix}$, and $\overline{\mathbf{B}} = \begin{pmatrix} \mathbf{I_{N-1}} \\ \mathbf{0_{3\times N-1}} \end{pmatrix}$.

From Equation 21, each of the soft segment curvatures can be directly controlled. The orientation of the tail and the planar position of the CoM with respect to the global coordinate system are indirectly controlled through the frictional interaction of the snake body with the ground.

Results

This section verifies the presented model through the comparison of numerical simulations with experimental results. The body of the soft robotic snake prototype comprises four bidirectional fluidic elastomer actuators as segments composed in series.

The experimental prototype is built through molding silicone rubber (Smooth-on Ecoflex 0030) following a fabrication process comprising three steps[21] as shown in Figure 4 and described below:

Step 1: Three premolds of the soft snake body are 3D printed. Two actuation premolds carry the negative of parallel rectangular fluidic channels connected on both ends in a serpentine arrangement. The third one is the constraint premold that has a thin rectangular opening with the same length and width as the channel layer.

Step 2: An inextensible flexible sheet is embedded into the constraint premold in order to add a constraint for the soft body to undergo bending deformation upon pressurization. Then, silicone rubber in poured into both premolds.

Step 3: When cured, all three molds are removed and two actuation molds are glued on both sides of the constraint mold using thin layers of uncured silicone rubber as glue.

The fluidic subsystem, the control subsystem, and the elastomeric body form the whole soft snake robot system. As a fluid source, we use a compressed air nozzle that provides a large pressure input, which passes through a regulator to obtain controlled pressure values compatible with our actuators, typically below 5 psi. The regulated pressure input is connected to a valve array that drives the soft snake robot. Each segment of the robot requires two valves to achieve bidirectional bending.

The aim of the control system is to move the snake robot in a way that follows the serpentine gait.[22] An NI-DAQ PCI 6009 transfers commands from Matlab to drive each valve. Eight digital outputs of the NI-6009 are used to control eight miniature solenoid valves, turning them on or off.

To verify our modeling approach, we performed simulations of the simplified soft snake robot dynamic model. The simulation adopts the ODE toolbox in Matlab to solve the differential equations of the soft snake robot model. Since solenoid valves switch between on and off positions, the dynamic response of fluidic elastomer actuators used as segments in our robot is also taken into account for step pressure inputs as shown in Figure 5.[22,23] Figure 6 displays simulation results including the initial and final positions of the snake body as well as the trajectory of the head. The following set of parameters were used in these simulations: $N=5$, $l_2=0.025$ m, $m=0.1$ kg, $U_t=0.1$, $U_n=0.9$. The gait of the snake is serpentine locomotion,[1] where the desired trajectory of each soft segment curvature is written as:

$$\kappa_i = \alpha \sin(\omega t + \beta_i), \tag{21}$$

where $i \in (1, \ldots, N-1)$ and ω and β_i are the frequency and phase offset of each angle; α is the curvature amplitude under a given input pressure value. In this demonstration of the model, the input pressure value, $P = 3.75$ psi, $\omega = \frac{2\pi}{3}$, and

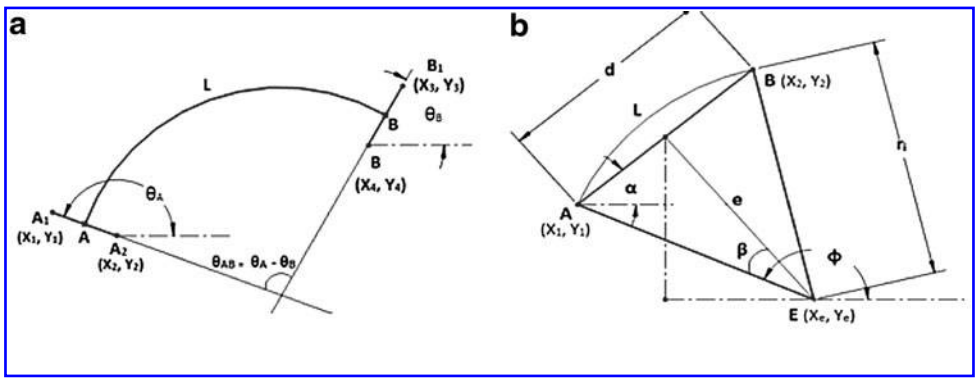

FIG. 8. Experimental information is processed for comparison with simulated results. **(a)** Curvature information is extracted from the positions and orientations of both ends of each segment. **(b)** The recovered segment shape when $r_i > 0$.

Algorithm 1 Segment curvature extraction

Require: Position of two points at each end of the segment:

A_1 (x_1, y_1), A_2 (x_2, y_2) and B_1 (x_3, y_3), B_2 (x_4, y_4)

Require: Segment length: l

1. The slope of point A: $\theta_A = \arctan\frac{(y_2 - y_1)}{(x_2 - x_1)}$
2. The slope of point B: $\theta_B = \arctan\frac{(y_4 - y_3)}{(x_4 - x_3)}$
3. The curvature of segment from A to B: $\kappa_i = \frac{\theta_A - \theta_B}{l}$

$\beta_i = 2\pi\frac{i}{N}$ rad/s. Figure 7 displays the position and velocity of the CoM of the soft snake robot for the same simulation.

To compare our model with experimental results, physical parameters of the snake robot prototype and the workspace were determined. Table 2 displays a list of measured parameters. We used a spring scale to measure the friction factors in two orthogonal directions (normal and tangential to the body axis) by recording the force from the spring scale as the robot began to move upon horizontal pulling. In addition, in order to measure the sliding friction in the normal direction, the passive wheels of the snake were fixed before the measurement. We repeated the measurements 10 times for both the tangential rolling friction and normal sliding friction cases. The mean friction coefficient values in tangential and normal directions were 0.0966 and 0.68, respectively, with standard deviations of 0.0015 and 0.01.

Experimental data are extracted using an external vision system. Positions of custom color markers placed at both ends of each segment (a total of 10 markers) are measured over time using an overhead camera and an open source visual tracking software.[24] Using two markers at each end of the segments, we can readily extract their average position and orientation, which were further processed in Matlab to calculate the curvature of each bending joint (segment) and the velocity of the CoM of the whole robot.

After an initial calibration of the tacking software, the position of each marker can be extracted with respect to the global coordinate frame. Based on the position and orientation information at both ends of each segment, we can calculate the curvature value as shown in Algorithm 1 and Figure 8. For comparison with the simulated snake body, Algorithm 2 and Figure 8 describe the recovery of the soft segment shape based on the extracted positions and calculated curvature values.

Therefore, using only marker positions obtained through visual feedback, these algorithms calculate the required information of the position, orientation, and shape of the soft robotic snake prototype. Figure 9 displays the recovered information overlaid with the original frame, following the snake motion in the experiment.

Based on image processing results, Figure 10 shows the curvature plot of each soft segment during an undulation experiment. There are four soft segments, which are shown with different curves in the figure. From this figure, the amplitudes and offsets of curvature waveforms of each soft segment are close but display variation, and the phase offsets between neighboring segments are also not constant. These variations are primarily because of small nonuniformities in fabrication, as well as variations in fluidic impedance between segments, surface flatness, and the effect of tubing. As a result, the snake robot has a tendency to move in a large circle instead of a straight line, which will be addressed via feedback control elsewhere.

In comparison, the simulated curvature plots of each soft segment are shown in Figure 11 using the same parameters

Algorithm 2 Recovery of the shape information of a soft segment

Require: Position of two points at each end of the segment:

A_1 (x_1, y_1), A_2 (x_2, $y2$) and B_1 (x_3, y_3), B_2 (x_4, y_4)

Require: Curvature of the segment: k_i

1. Position of point A: $A(x_A, y_A) = (\frac{x_1 + x_2}{2}, \frac{y_1 + y_2}{2})$
2. Position of point B:$B(x_B, y_B) = (\frac{x_3 + x_4}{2}, \frac{y_3 + y_4}{2})$
3. The radius of curvature of the segment: $r_i = \frac{1}{k_i}$
4. The angle of the line AB: $\alpha = \arctan(\frac{y_B - y_A}{x_B - x_A})$
5. The midpoint position between A and B: $x_c = \frac{x_A + x_B}{2}, y_c = \frac{y_A + y_B}{2}$
6. The distance between A and B: $d = \sqrt{(x_B - x_A)^2 + (y_B - y_A)^2}$
7. The half arc-angle: $\beta = \arcsin\frac{d/2}{r_i}$
8. The distance between the midpoint and the center of curvature point is $e = \sqrt{(r_i^2 - \frac{d^2}{4})}$
9. **If** $r_i = 0$ **then**
10. Draw a straight line between point **A** and **B**
11. **else if** $r_i > 0$ **then**
12. The center of curvature point **E** position $x_e = x_c + e\sin(\alpha), y_e = y_c - e\cos(\alpha)$
13. The angles of lines **EA, EB** are $\phi_A = \frac{\pi}{2} + \alpha + \beta, \phi_B = \frac{\pi}{2} + \alpha - \beta$
14. Draw the arc based on the equations $x = x_e + r_i\cos(\phi_{AB}), y = y_e - r_i\sin(\phi_{AB}), \phi_{AB} = \phi_A : \phi_B$
15. **else if** $r_i > 0$ **then**
16. The center of curvature point **E** position $x_e = x_c - e\sin(\alpha), y_e = y_c + e\cos(\alpha)$
17. The angles of lines **EA, EB** are $\phi_A = \frac{\pi}{2} + \alpha - \beta, \phi_B = \frac{\pi}{2} + \alpha + \beta$
18. Draw the arc based on the equations $x = x_e + r_i\cos(\phi_{AB}), y = y_e - r_i\sin(\phi_{AB}), \phi_{AB} = \phi_A : \phi_B$
19. **end if**

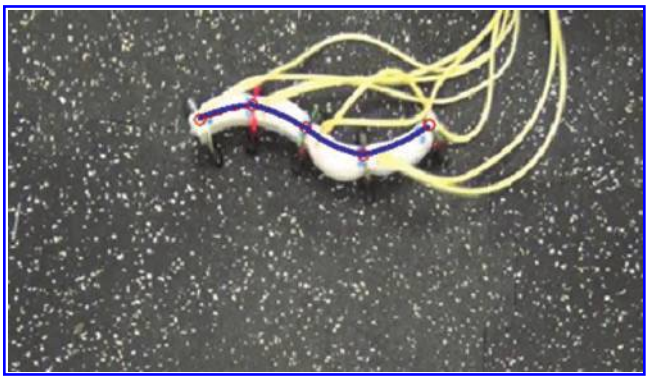

FIG. 9. The overlaid curve on the soft snake robot indicates the recovered shape and position of the snake from visual feedback. Color images available online at www.liebertpub.com/soro

as for the experiments. These curves display approximate sinusoidal waveforms, as square wave pressure inputs are smoothened by the segment dynamics.

Experimental curvature measurements are directly compared to simulation results in Figure 12 for all segments. Dashed lines represent simulations, and solid lines represent experimental results. All $N-1$ curvatures can be directly controlled by independent pressure inputs in a similar manner by switching solenoid valves and relying on the segment dynamics. These curves indicate a good match between model predictions and experimental results.

To compare the simulated and experimental shape of the snake robot over time, we adopted a local frame method. Placing a coordinate system at the CoM of the snake robot with zero heading angle (defined as the average orientation of the body), we achieved a standard way to focus only on the shape information. Figure 13 shows the shape of the soft snake robot body for both the experiment (solid) and the simulation (dashed) on the same plane at four sample points in time.

The root-mean-square (RMS) error caused by the shape differences between the theoretical model prediction and experimental measurements during the whole motion is displayed in Figure 14. The total length of our snake robot is 0.24 m and the mean RMS error is 0.0138 m, approximately 5.75% of the body length, indicating good accuracy. There are a number of experimental sources of error in the body shape. The snake robot is expected to follow a straight line,

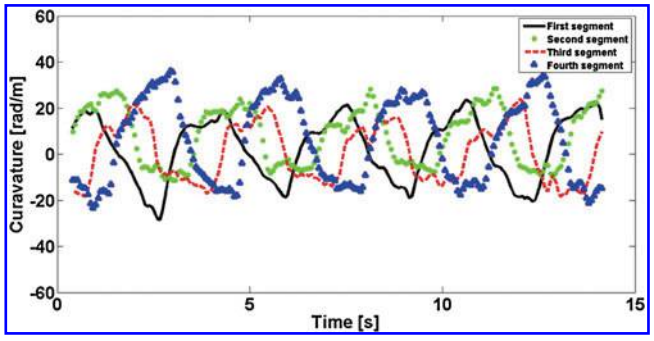

FIG. 10. The curvature plot of each soft segment in the experiment. The solid line, circle, dashed line, and triangle represent the 1st, 2nd, 3rd, and 4th soft segments, respectively. Color images available online at www.liebertpub.com/soro

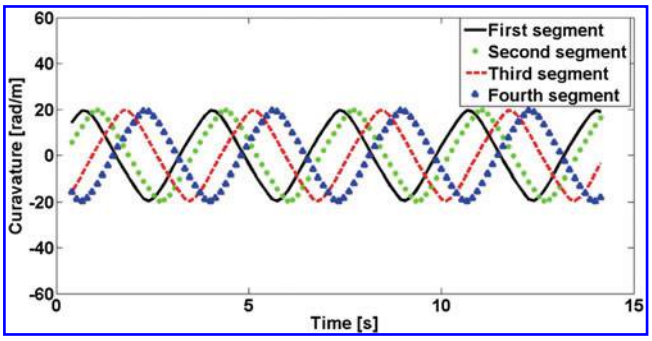

FIG. 11. The curvature plot of each soft segment in the simulation. The solid line, circle, dashed line, and triangle represent the 1st, 2nd, 3rd, and 4th soft segments, respectively. Color images available online at www.liebertpub.com/soro

but turns slightly during locomotion; curvature amplitudes are not constant among segments; tubings cause external force; and the constraint layer is not located precisely in the middle of the body.

Linear velocity of the snake robot is determined by the CoM position over time. Noise in experimental results was reduced using a moving line fit around the current point in time. With a 15 fps camera feed, we used the position information from five frames before and after the current frame and used the slope of the best fit line as the extracted velocity. This method reduced oscillations caused by tracking pixel variations between segments while not inducing lag. Figure 15 displays the velocities of the CoM for the snake robot from both experimental (solid) and simulation (dashed) results. From this figure, a periodicity of velocity is observed around a similar average linear velocity, in line with our model predictions.

Figure 16 shows the rotational angle of the tail for simulated (dashed) and experimental (solid) results. Please note that this angle cannot be directly controlled. If the snake robot follows a straight line in a global coordinate, then the sum of all rigid link angles should be equal to 0.[7] Hence, this uncontrolled value provides a good indicator of the overall orientation of the robot body over time. For no rotation, the tail angle should oscillate around a constant offset value with no linear change with time, which is the case for the simulation results. However, in the experiment, the snake turns over time, indicated by a drift in the tail angle offset.

To evaluate the strength of the model to describe the behavior of our soft robotic snake, we performed a comparison of simulation and experimental results within the feasible operational parameters of the driving frequency of the curvature waveform in Equation 22 and pressure input values, which are directly related to the curvature amplitudes in Equation 22. The resulting CoM velocities for each of these parameter combinations are shown in Figure 17 as contour plots for the simulated model predictions and experimental results. Pressure is ranged from 3.125 to 5 psi and the frequency is ranged from 0.16 to 1.5 Hz. The results confirm that the model predictions are in line with experimental observations, subject to associated uncertainties.

Two cases of parameter combinations are not investigated. Low-frequency and high-pressure case would build up too much pressure in the actuators for a long period causing potential rupture. High-frequency and low-pressure case immobilizes the snake robot since the incoming fluid is

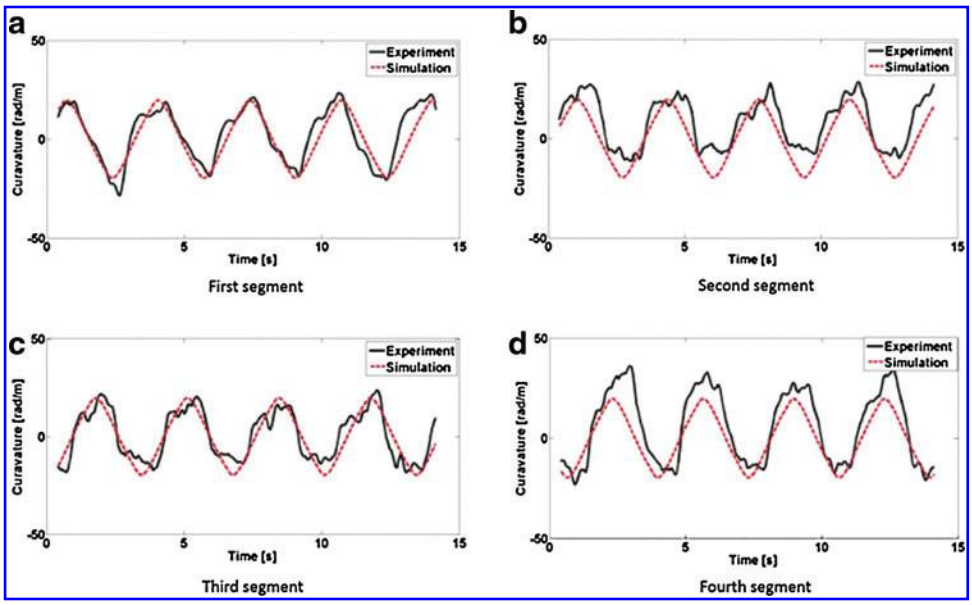

FIG. 12. Curvature waveforms of each segment in the experiment (solid line) and the simulation (dashed line). Color images available online at www.liebertpub.com/soro

released quickly before deformation can be observed. Simulations generated combinations of 56 frequency and 31 pressure values within the given ranges. We performed each experiment three times and removed any outliers before calculating the average values. The information between the measurement points is extracted through interpolation.

We also tested the dynamic parameter values of the actuators for each pressure input. The behavior of the soft actuator looks like a second-order system:

$$\kappa = C_0 + C_1 e.^{-t/\tau_1} + C_2 e^{-t/\tau_2}, \tag{22}$$

where κ is the curvature of the actuator, τ_1 and τ_2 are the time constants, C_0, C_1 and C_2 are constant coefficients. This is a reasonable assumption from circuit equivalence, since the channels inside the soft actuators act both as a capacitance and an impedance, and the pneumatic tubing acts as an impedance creating a second-order dynamic system as we verified previously by Onal and Rus.[22]

On the basis of this analysis, the CoM velocity increases with increasing input pressure for a fixed frequency until the input pressure reaches a saturation level approaching a maximum bending amplitude, which leads to a similar response in the CoM velocity. For a fixed pressure input, we observed an optimal frequency that maximizes speed.[22,23] The ability of the model to describe the performance of the robot under different conditions motivates future research on design and parameter optimization based on different

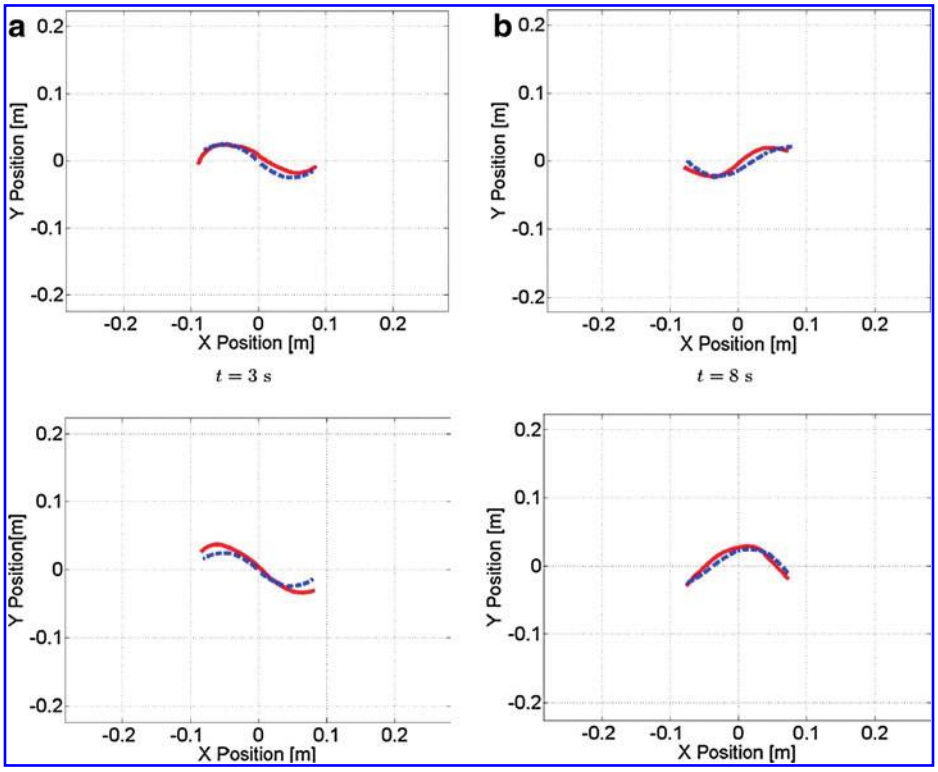

FIG. 13. Comparison of the snake robot shapes between the simulation and the experiment at 3, 8, 13, and 16 s. The dashed line shows the simulation and the solid line shows the experimental results. Color images available online at www.liebertpub.com/soro

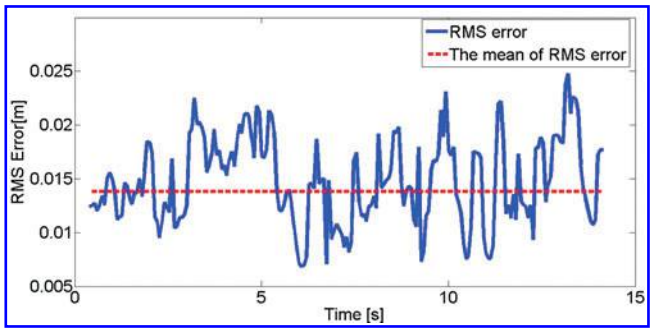

FIG. 14. The root-mean-square (RMS) error of the shape difference between the experiment and the simulation. Color images available online at www.liebertpub.com/soro

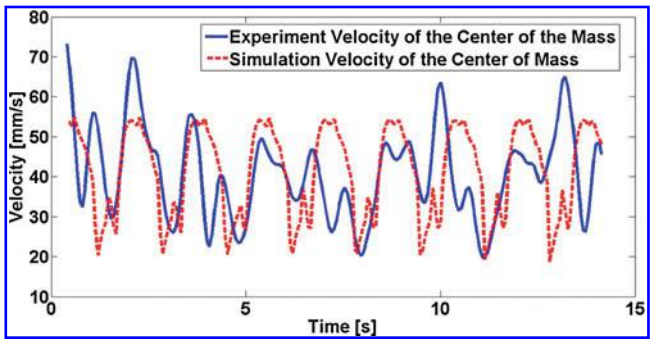

FIG. 15. The velocities of the CoM of the snake robot in simulation (dashed line) and the experiment (solid line). Color images available online at www.liebertpub.com/soro

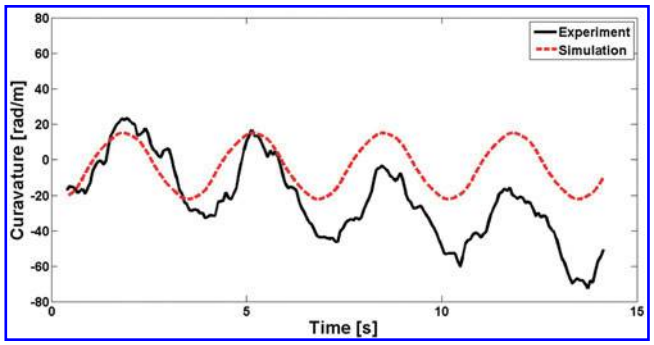

FIG. 16. The angular orientation of the last rigid point (tail) of the snake robot in the experiment (solidline) and the simulation (dashed line). Color images available online at www.liebertpub.com/soro

types of actuators,[25] friction factors, and geometric parameters.

Conclusion

This article presented a theoretical dynamic model of a soft snake robot made of silicone rubber, provided simulation results, and verified the effectiveness of the model through a detailed comparison with experimental results on the locomotion of the robot on a surface. The fundamental approach we take in this modeling study is applicable to most pressure-operated soft robots we develop by a modular kinematic arrangement of bending-type fluidic actuators embedded in elastomers.

This work represents our first step to develop rigorous theoretical studies on fluidic elastomer robots. Based on the presented dynamic model, future studies on soft robots can implement advanced theoretical optimization,[26] control, navigation, planning, and learning algorithms similar to their rigid counterparts.[5,27]

Differences between theoretical predictions and experimental results were investigated through data analysis and found to be acceptable without feedback control. However, in order to complete specific tasks precisely, low-level feedback control will be a necessity. Thus, we are studying soft curvature sensors compatible with our soft robot fabrication process to close the loop.

Reducing external disturbances, especially caused by tubing connections, is another future research direction. Reliability and repeatability in manufacturing our soft robotic snake will be addressed in next-generation designs. Another future goal is to eliminate the passive wheels, which create the necessary frictional anisotropy required for serpentine locomotion. Most snake robots use this technique to slide on the ground more freely along the tangential axis than the normal axis. For real-world unstructured environments, wheels may not be the best solution. A soft robotic snake may be more suitable to eliminate wheels and use a skin similar to its natural counterpart because of its compliance and weight benefits. We aim to develop an artificial skin for the next-generation of our soft robotic snake.[28]

Since a soft robot body is safer than a rigid one, our current work is suitable for search and rescue, medical, and manufacturing applications. The theoretical modeling study described in this article will be extended to a 3D workspace in order to move and control a 3D soft manipulator toward the mentioned applications.[29–31]

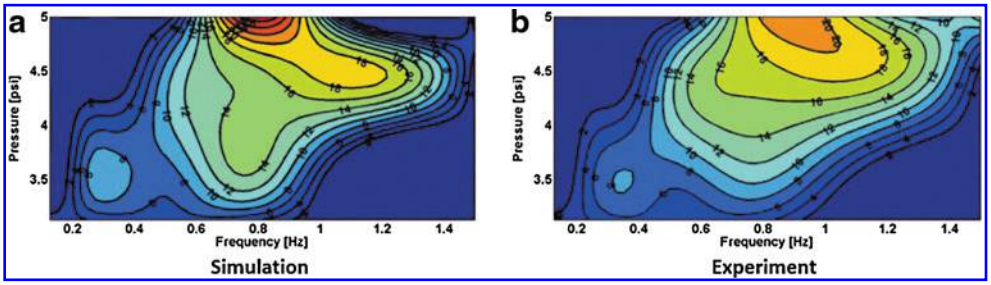

FIG. 17. Comparison of model predictions and experimental results for different operational parameters of the soft robotic snake in terms of resulting CoM velocities. Contour plots of the linear velocity of the robot CoM with varying frequencies from 0.16 to 1.5 Hz (*x*-axis) and pressure inputs ranging from 3.125 to 5 psi (*y*-axis) are displayed for simulation **(a)** and experimental **(b)** results. The CoM velocity levels are stepped at 2 mm/s, annotated on the curves, and indicated as color coding from blue to red. Color images available online at www.liebertpub.com/soro

Author Disclosure Statement

No competing financial interests exist.

References

1. Hirose S. Biologically Inspired Robots: Snake-like Locomotors and Manipulators. Oxford: Oxford University Press, 1993.
2. SINTEF. Available at www.sintef.no/home/Information-and-CommunicationTechnology-ICT/Applied-Cybernetics/Projects/Our-snake-robots/
3. McKenna JC, Anhalt DJ, Bronson FM, Brown HB, Schwerin M, Shammas E, Choset H. Toroidal skin drive for snake robot locomotion. In: Proceedings of the IEEE International Conference on Robotics and Automation (ICRA), 2008, pp. 1150–1155.
4. Sato M, Fukaya M, Iwasaki T. Serpentine locomotion with robotic snakes. IEEE Control Syst 2002;22:64–81.
5. Fjerdingen SA, Mathiassen J, Schumann-Olsen H, Kyrkjeb E. Adaptive snake robot locomotion: a benchmarking facility for experiments. In: Proceedings of the European Robotics Symposium. New York: Springer, 2008, pp. 13–22.
6. Shugen M, Naoki T. Analysis of creeping locomotion of a snake-like robot. Adv Robot 2001;15:205–224.
7. Pettersen KY, Stavdahl Ø, Gravdahl JT. Snake Robots: Modelling, Mechatronics, and Control. New York: Springer, 2013.
8. Matsuno F, Suenaga K. Control of redundant 3D snake robot based on kinematic model. In: Proceedings of the IEEE International Conference on Robotics and Automation (ICRA), Vol. 2, 2003, pp. 2061–2066.
9. Tanaka M, Matsuno F. Control of 3-dimensional snake robots by using redundancy. In: Proceedings of the IEEE International Conference on Robotics and Automation (ICRA), 2008, pp. 1156–1161.
10. Transeth AA, Leine RI, Glocker C, Pettersen KY. 3-D snake robot motion: non-smooth modeling, simulations, and experiments. IEEE Trans Robot 2008;24:361–376.
11. Trimmer BA, Lin H-T, Baryshyan A, Leisk GG, Kaplan DL. Towards a biomorphic soft robot: design constraints and solutions. In: Proceedings of the IEEE 4th IEEE RAS & EMBS International Conference on Biomedical Robotics and Biomechatronics (BioRob), 2012, pp. 599–605.
12. Menciassi A, Gorini S, Pernorio G, Weiting L, Valvo F, Dario P. Design, fabrication and performances of a biomimetic robotic earthworm. In: Proceedings of the IEEE International Conference on Robotics and Biomimetics (ROBIO), 2004, pp. 274–278.
13. Morin SA, Shepherd RF, Kwok SW, Stokes AA, Nemiroski A, Whitesides GM. Camouflage and display for soft machines. Science 2012;337:828–832.
14. Wright C, Buchan A, Brown B, Geist J, Schwerin M, Rollinson D, Tesch M, Choset H. Design and architecture of the unified modular snake robot. In: Proceedings of the IEEE International Conference on Robotics and Automation (ICRA), 2012, pp. 4347–4354.
15. Wright C, Johnson A, Peck A, McCord Z, Naaktgeboren A, Gianfortoni P, Gonzalez-Rivero M, Hatton R, Choset H. Design of a modular snake robot. In: Proceedings of the IEEE/RSJ International Conference on Intelligent Robots and Systems (IROS), 2007, pp. 2609–2614.
16. Trimmer BA, Takesian AE, Sweet BM, Rogers CB, Hake DC, Rogers DJ. Caterpillar locomotion: a new model for soft-bodied climbing and burrowing robots. In: Proceedings of the 7th International Symposium on Technology and the Mine Problem, Vol. 1, 2006, pp. 1–10.
17. Shepherd RF, Ilievski F, Choi W, Morin SA, Stokes AA, Mazzeo AD, Chen X, Wang M, Whitesides GM. Multigait soft robot. Proc Natl Acad Sci USA 2011;108:20400–20403.
18. Biagiotti L, Melchiorri C, Tiezzi P, Vassura G. Modelling and identification of soft pads for robotic hands. In: Proceedings of the IEEE/RSJ International Conference on Intelligent Robots and Systems (IROS), 2005, pp. 2786–2791.
19. Xydas N, Bhagavat M, Kao I. Study of soft-finger contact mechanics using finite elements analysis and experiments. In: Proceedings of the IEEE International Conference on Robotics and Automation (ICRA), Vol. 3, 2000, pp. 2179–2184.
20. Ilievski F, Mazzeo AD, Shepherd RF, Chen X, Whitesides GM. Soft robotics for chemists. Angew Chem 2011;123:1930–1935.
21. Onal CD, Rus D. A modular approach to soft robots. In: Proceedings of the IEEE RAS & EMBS International Conference on Biomedical Robotics and Biomechatronics (BioRob), 2012, pp. 1038–1045.
22. Onal CD, Rus D. Autonomous undulatory serpentine locomotion utilizing body dynamics of a fluidic soft robot. Bioinspir Biomim 2013;8:026003.
23. Luo M, Agheli M, Onal CD. Theoretical modeling of a pressure-operated soft snake robot. In: Proceedings of the International Design and Engineering Technical Conferences & Computers and Information in Engineering Conference (IDETC/CIE 2014). In press.
24. Brown D. Tracker video analysis and modeling tool. Available at http://www.cabrillo.edu/dbrown/tracker/
25. Luo M, Tao W, Chen F, Khuu TK, Ozel S, Onal CD. Design improvements and dynamic characterization on fluidic elastomer actuators for a soft robotic snake. In: Proceedings of the IEEE International Conference on Technologies for Practical Robot Applications, 2014. TePRA 2014. In press.
26. Kalani H, Akbarzadeh A, Bahrami H. Application of statistical techniques in modeling and optimization of a snake robot. Robotica 2012;1:1–19.
27. Dehghani M, Mahjoob MJ. A modified serpenoid equation for snake robots. In: Proceedings of the IEEE International Conference on Robotics and Biomimetics (ROBIO), 2009, pp. 1647–1652.
28. Marvi H, Hu DL. Friction enhancement in concertina locomotion of snakes. J R Soc Interface 2012;9:3067–3080.
29. Ranzani T, Cianchetti M, Gerboni G, De Falco I, Petroni G, Menciassi A. A modular soft manipulator with variable stiffness. 3rd Joint Workshop on New Technologies for Computer/Robot Assisted Surgery, 2013.
30. Laschi C, Cianchetti M, Mazzolai B, Margheri L, Follador M, Dario P. Soft robot arm inspired by the octopus. Adv Robot 2012;26:709–727.
31. Liljeback P, Stavdahl O, Pettersen KY. Modular pneumatic snake robot: 3d modelling, implementation and control. Model Identif Control 2008;29:21–28.

Address correspondence to:
Ming Luo
Robotics Engineering Program
Worcester Polytechnic Institute
100 Institute Road, Higgins Labs 130
Worcester, MA 01609

E-mail: mluo@wpi.edu